Inorganic Chemistry
Cite This: Inorg. Chem. XXXX, XXX, XXX–XXX
Article
pubs.acs.org/IC

Novel and Versatile Imine-N-Heterocyclic Carbene Half-Sandwich Iridium(III) Complexes as Lysosome-Targeted Anticancer Agents

Yuliang Yang,[†] Lihua Guo,*[,†] Zhenzhen Tian,[†] Yuteng Gong,[†] Hongmei Zheng,[†] Shumiao Zhang,[†] Zhishan Xu,[†,‡] Xingxing Ge,[†] and Zhe Liu*[,†]

[†]Institute of Anticancer Agents Development and Theranostic Application, The Key Laboratory of Life-Organic Analysis and Key Laboratory of Pharmaceutical Intermediates and Analysis of Natural Medicine, Department of Chemistry and Chemical Engineering, Qufu Normal University, Qufu 273165, China

[‡]Department of Chemistry and Chemical Engineering, Shandong Normal University, Jinan 250014, China

Supporting Information

ABSTRACT: We, herein, report the synthesis, characterization, luminescence properties, anticancer, and antibacterial activities of a family of novel half-sandwich iridium(III) complexes of the general formula $[(\eta^5\text{-}Cp^x)Ir(C\text{^}N)Cl]PF_6^-$ [Cp^x = pentamethylcyclopentadienyl (Cp*) or tetramethyl(biphenyl)-cyclopentadienyl (Cp^{xbiph})] bearing versatile imine-N-heterocyclic carbene ligands. In this complex framework, substituents on four positions could be modulated, which distinguishes this class of complex and provides a large amount of flexibility and opportunity to tune the cytotoxicity of complexes. The X-ray crystal structures of complexes **4** and **10** exhibit the expected "piano-stool" geometry. With the exception of **1**, **2**, and **11**, each complex shows potent cytotoxicity, with IC_{50} (half-maximum inhibitory concentration) values ranging from 1.99 to 25.86 μM toward A549 human lung cancer cells. First, the effect of four positions bearing different substituents in the complex framework on the anticancer activity, that is, structure–activity relationship, was systematically studied. Complex **8** (IC_{50} = 1.99 μM) displays the highest anticancer activities, whose cytotoxicity is more than 10-fold higher than that of the clinical platinum drug cisplatin against A549 cancer cells. Second, their chemical reactivity including nucleobases binding, catalytic activity in converting coenzyme NADH to NAD^+, reaction with glutathione (GSH), and bovine serum albumin (BSA) binding is investigated. No reaction with nucleobase is observed. However, these iridium(III) complexes bind rapidly to GSH and can catalyze oxidation of NADH to NAD^+. In addition, they show moderate binding affinity to BSA and the fluorescence quenching of BSA by the iridium (III) complexes is due to the static quenching. Third, the mode of cell death was also explored through flow cytometry experiments, including cell cycle, apoptosis induction, reactive oxygen species (ROS) and mitochondrial membrane potential. It seems that cell cycle perturbation, apoptosis induction, increase of ROS level and loss of mitochondrial membrane potential together contribute to the anticancer potency of these complexes. Last, the use of confocal microscopy provides insights into the microscopic mechanism that the typical and most active complex **8** enters A549 lung cancer cells mainly through energy-dependent pathway and is located in lysosome. Furthermore, lysosome damage and nuclear morphology were detected by confocal microscopy. Nuclear condensation and apoptotic bodies may finally induce cells apoptosis. Interestingly, complex **8** also shows antibacterial activity against Gram-positive *Staphylococcus aureus*. This work may provide an alternative and effective strategy to smart design of potent organometallic half-sandwich iridium(III) anticancer drugs.

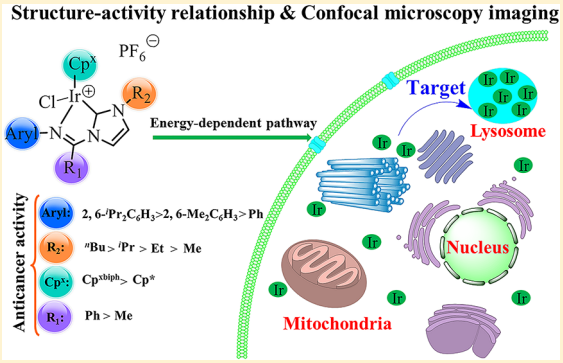

INTRODUCTION

The N-heterocyclic carbenes (NHCs) have been proved to be the efficient ancillary ligands because of their strong coordination ability and easily tunable structure by the steric and electronic substituents on the metal center.[1] Most of the transition metals from group 7 to group 11 in the periodic table can be coordinated by the NHC ligands.[1h,2] Metal complexes bearing different NHC ligands have been prepared and employed in various fields, particularly as catalysts and anticancer agents.[1h,3] Among these ligands, imine-N-heterocyclic carbene is an attractive class of chelating ligands that combine a hard-donor imine group with the soft-donor properties of an NHC.[4]

The successful application of platinum-based anticancer agents in the clinical has stimulated the research for other metal-based diagnostic drugs and chemotherapeutic drugs, which may be able to diminish severe toxic side effects, overcome platinum resistance, and broaden the spectrum of sensitive tumors.[5] For metal-based chemotherapeutic drugs, both metal ions and the nature of chelating ligands play key

Received: June 15, 2018

Downloaded from pubs.acs.org by UNIV OF WINNIPEG on 08/23/18. For personal use only.
Inorg. Chem.

© XXXX American Chemical Society

DOI: 10.1021/acs.inorgchem.8b01656
Inorg. Chem. XXXX, XXX, XXX–XXX

roles in the therapeutic efficiency of anticancer agents.[6] Recently, a series of highly potent half-sandwich organometallic anticancer agents bearing different chelating ligands, such as bis-NHC ligands, imine-pyridyl ligands, and pyridyl-NHC ligands (Scheme 1), have been reported.[6,7] Our group

Scheme 1. Reported Half-Sandwich Anticancer Complexes and Our Current Work

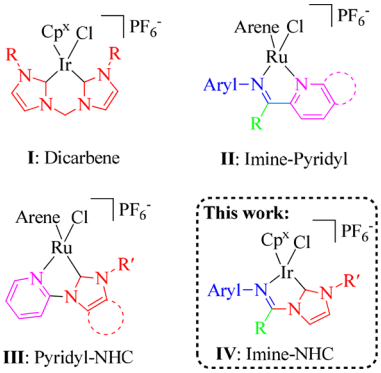

have developed a series of half-sandwich iridium(III) complexes containing bis-NHC ligands (**I**, Scheme 1).[7a] These complexes exhibit potent cytotoxicity toward HeLa human cervical cancer cells, and the anticancer activity of these complexes can be tuned by varying substitutions at two different interior positions. Our group has also synthesized a class of imine-pyridyl half-sandwich iridium(III) and ruthenium(II) complexes (**II**, Scheme 1).[6,7b] The cytotoxicity and cancer cell selectivity of such complexes can be governed via alternative metal ions and chelating ligands around the metal. Recently, Hartinger et al. designed some pyridyl-NHC organoruthenium anticancer complexes (**III**, Scheme 1) and studied their antiproliferative properties and reactions with biomolecules.[7c] In this system, introduction of different substituents gave complexes with a wide variety of properties. These results encouraged us to prepare a series of half-sandwich iridium(III) complexes bearing imine-N-heterocyclic carbene chelating ligands and explore their anticancer activity and reactivity toward biomolecules.

Moreover, confocal microscopy imaging has achieved a great success in the field of biology and medicine.[8] It has a lot of advantages, such as higher resolution than conventional optical microscopes, enabling continuous nondestructive optical sectioning of samples, removing the influence of stray light, and increasing the clarity of the image. The development of fluorescent anticancer complexes can help researchers to real-time track drug intracellular transport and distribution in cells, and to monitor the interactions between the drug and the biological target molecule, thus providing an important tool for exploring the mechanism of actions (MoAs) of the anticancer drugs. Cyclometalated iridium(III) or ruthenium(II) anticancer complexes have been widely used as imaging agents and probes by virtue of their intense emission, long emission lifetimes, large Stokes shifts, and high photo stability.[9] However, half-sandwich anticancer iridium(III) complexes used for confocal microscopy imaging have been rarely reported.

In this contribution, 12 novel half-sandwich iridium(III) complexes of the form $[(\eta^5\text{-Cp}^x)\text{Ir(C^N)Cl}]\text{PF}_6$, where C^N are imine N-heterocyclic carbene ligands with different substituents, have been prepared and fully characterized. In this C^N-ligand framework, three positions of the ligand could be modulated, respectively, which distinguishes this class of ligand and provides a large amount of flexibility and opportunities to tune the cytotoxicity of such complexes. These complexes have been systematically investigated for their chemical and biological reactivity, cancer cell toxicity against A549 cancer cells, antibacterial activity against *Staphylococcus aureus* (*S. aureus*) and molecular imaging in live cells. On the basis of these studies, we tried to understand the mechanism of actions of these iridium(III) complexes. The results demonstrated that this type of iridium(III) complexes has a great potential in cancer chemotherapy.

RESULTS AND DISCUSSION

Synthesis, Characterization, and Spectroscopic Properties. The synthetic routes to imine-N-heterocyclic carbene ligands **L1−L11** and novel half-sandwich iridium(III) complexes **1−12** are depicted in Scheme 2. A series of

Scheme 2. Synthetic Routes for Imine-N-Heterocyclic Carbene Ligands L1−L11 and $[(\eta^5\text{-Cp}^x)\text{Ir(C^N)Cl}]\text{PF}_6$ Complexes 1−12

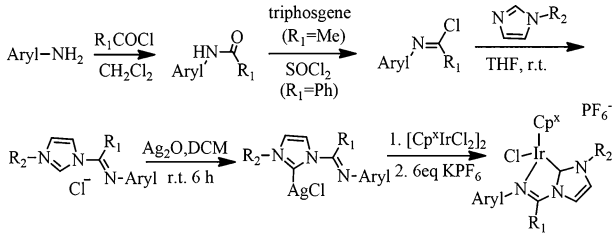

Complex	Cp^x	Aryl	R_1	R_2	Complex	Cp^x	Aryl	R_1	R_2
1	Cp*	2,6-$Me_2C_6H_3$	Me	Me	**7**	Cp*	2,6-$^i Pr_2C_6H_3$	Me	^{i}Pr
2	Cp*	2,6-$Me_2C_6H_3$	Me	Et	**8**	Cp*	2,6-$^i Pr_2C_6H_3$	Me	^{n}Bu
3	Cp*	2,6-$Me_2C_6H_3$	Me	^{i}Pr	**9**	Cp*	2,6-$Me_2C_6H_3$	Ph	^{i}Pr
4	Cp*	2,6-$Me_2C_6H_3$	Me	^{n}Bu	**10**	Cp*	2,6-$Me_2C_6H_3$	Ph	^{n}Bu
5	Cp*	2,6-$^i Pr_2C_6H_3$	Me	Me	**11**	Cp*	Ph	Ph	^{i}Pr
6	Cp*	2,6-$^i Pr_2C_6H_3$	Me	Et	**12**	Cp^{xbiph}	2,6-$Me_2C_6H_3$	Me	Me

imidazolium salts (C^imine·HCl) (**L1−L11**) containing different substituents were synthesized in good yields by a coupling reaction of the corresponding imidoyl chlorides with imidazole bearing the different substituents. Novel half-sandwich iridium(III) complexes **1−12** were synthesized in high yields (75−97%) via the classical transmetalation method. All the synthesized iridium(III) complexes were isolated as PF_6^- salts and fully characterized by ^{1}H NMR spectroscopy (Figures S1−S12), CHN elemental analysis, ESI-MS (Figures S13−S33), and X-ray crystallography.

Due to the similarity in the structure of these complexes, the complex **8** was selected as a representative complex to monitor spectroscopic properties. First, the UV−vis absorption of the complex **8** in CH_3CN solution was determined utilizing UV spectrophotometer. As seen from Figure 1a, a weak absorption peak at ∼320 nm was detected. Next, as illustrated in Figure 1b, the maximum emission wavelengths of the complex **8** were conducted by fluorescence spectroscopy, which were at 503 and 565 nm when excited at 322 nm. The emission spectrum of complex **8** located at 565 nm was dominated.

X-ray Crystal Structures. The X-ray crystal structures of complexes $[(\eta^5\text{-}C_5Me_5)\text{Ir(L4)Cl}]\text{PF}_6^-$ (**4**) and $[(\eta^5\text{-}C_5Me_5)$-

DOI: 10.1021/acs.inorgchem.8b01656
Inorg. Chem. XXXX, XXX, XXX−XXX

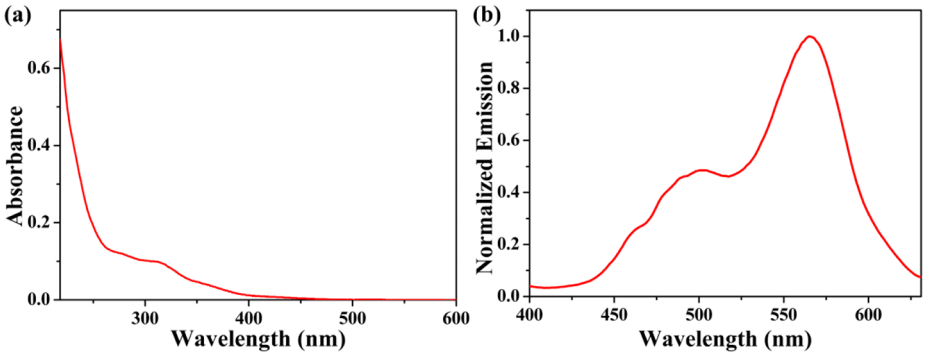

Figure 1. UV−vis absorption spectra (a) and fluorescence spectra of (b) of complex **8** in CH_3CN solution (20 μM).

Ir(L10)Cl]PF_6^- (**10**) were unambiguously confirmed and their molecular structures are shown in Figure 2. X-ray crystallo-

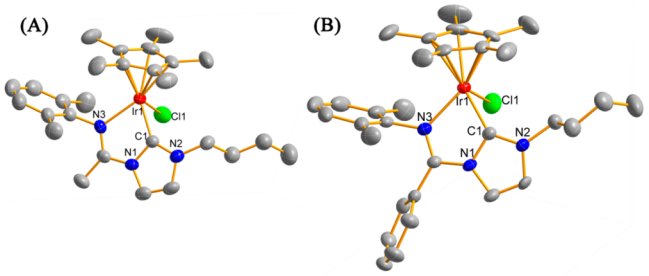

Figure 2. X-ray crystal structures of compounds of (A) [(η^5-C_5Me_5)Ir(L4)Cl]PF_6^- (**4**) and (B) [(η^5-C_5Me_5)Ir(L10)Cl]PF_6^- (**10**) with the thermal ellipsoids drawn at the 50% probability level. The hydrogen atoms and PF_6^- counterions have been omitted for clarity. Selected bond lengths (Å) and angles (deg): complex **4** Ir−C(centroid) = 1.8372, Ir−$C_{carbene}$ = 2.006(4), Ir−N = 2.131(4), Ir−Cl = 2.4036(13), $C_{carbene}$−Ir−N = 75.53(16), $C_{carbene}$−Ir−Cl = 82.39(14), N−Ir−Cl = 89.58(11); complex **10** Ir−C(centroid) = 1.8392, Ir−$C_{carbene}$ = 2.009(5), Ir−N = 2.135(5), Ir−Cl = 2.4009(15), $C_{carbene}$−Ir−N = 76.2(2), $C_{carbene}$−Ir−Cl = 80.97(17), N−Ir−Cl = 88.65(13).

graphic data are listed in Table S2, and selected bond lengths and angles are summarized in Table S3. Complexes **4** and **10** are arranged in monoclinic crystal systems with the *C*2/*c* and *P*2(1)/*c* space group, respectively. Each complex adopts the expected half-sandwich distorted-octahedral "three-legged piano-stool" geometry. The distance between the iridium(III) center and the centroid of Cp* (pentamethylcyclopentadienyl) ring is 1.8372 and 1.8392 Å for **4** and **10**, respectively.

Study of the Structure−Activity Relationship. The in vitro cytotoxicity of complexes **1**−**12** and cisplatin toward A549 cancer cells was determined after a 24 h exposure period using the MTT assay.[10] Although these iridium(III) complexes possess very similar structures, they have different anticancer activities. Subtle changes in the framework of such complexes result in a significant change on their biological behaviors. As depicted in Table 1 and Figure 3, the resulting 50% growth inhibitory concentration (IC_{50}) values for the complexes **1**, **2**, and **11** were >100 μM and thus deemed as inactive. However, other nine complexes display promising activity toward A549 cancer cells comparable to or even higher than cisplatin. Notably, an especially high anticancer activity is showed for complexes **7** and **8**. They give a ∼10-fold increase in cytotoxic potency than that of cisplatin against A549 cells. On the whole, the in vitro anticancer activities of these complexes revealed

Table 1. Inhibition of the Growth of A549 Cancer Cells by Complexes 1−12 and Cisplatin[a]

complex	IC_{50} (μM)
[(η^5-Cp*)Ir(L1)Cl]PF_6 (**1**)	>100
[(η^5-Cp*)Ir(L2)Cl]PF_6 (**2**)	>100
[(η^5-Cp*)Ir(L3)Cl]PF_6 (**3**)	25.86 ± 1.2
[(η^5-Cp*)Ir(L4)Cl]PF_6 (**4**)	14.05 ± 0.1
[(η^5-Cp*)Ir(L5)Cl]PF_6 (**5**)	9.15 ± 0.2
[(η^5-Cp*)Ir(L6)Cl]PF_6 (**6**)	3.04 ± 0.5
[(η^5-Cp*)Ir(L7)Cl]PF_6 (**7**)	2.21 ± 0.2
[(η^5-Cp*)Ir(L8)Cl]PF_6 (**8**)	1.99 ± 0.1
[(η^5-Cp*)Ir(L9)Cl]PF_6 (**9**)	3.94 ± 0.3
[(η^5-Cp*)Ir(L10)Cl]PF_6 (**10**)	3.64 ± 0.3
[(η^5-Cp*)Ir(L11)Cl]PF_6 (**11**)	>100
[(η^5-[b]Cp^{xbiph})Ir(L1)Cl]PF_6 (**12**)	7.44 ± 0.3
cisplatin	21.30 ± 1.7

[a]IC_{50} (half-maximum inhibitory concentration) values are drug concentrations necessary for 50% inhibition of cell viability. Data are presented as means ± standard deviations and cell viability is assessed after 24 h of incubation. [b]Cp^{xbiph} = tetramethyl(biphenyl)-cyclopentadienyl.

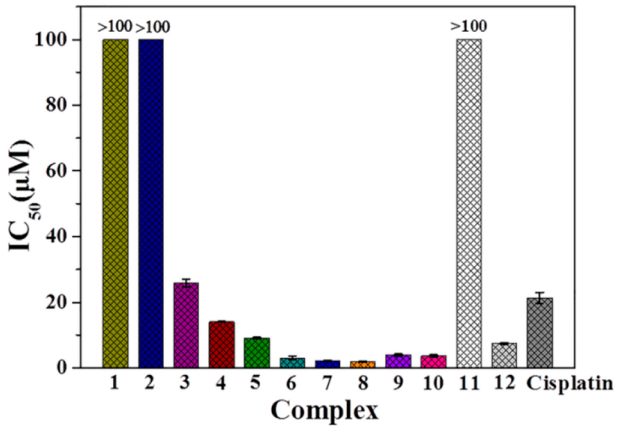

Figure 3. Inhibition of the growth of A549 cells by complexes **1**−**12** and cisplatin.

the following trends: **8** ≈ **7** ≈ **6** > **12** > **10** > **9** > **5** > **4** > cisplatin > **3**.

First, the steric hindrance of ortho-substituents in the aniline shows a significant effect on the cytotoxicity of complexes. Replacement of the aniline substituents from 2,6-dimethyl to 2,6-diisopropyl results in an excellent increase in anticancer activity. For example, complexes **5**, **6**, **7**, and **8**, whose IC_{50} values are 9.15, 3.04, 2.21, and 1.99 μM, respectively, exhibit in

DOI: 10.1021/acs.inorgchem.8b01656
Inorg. Chem. XXXX, XXX, XXX−XXX

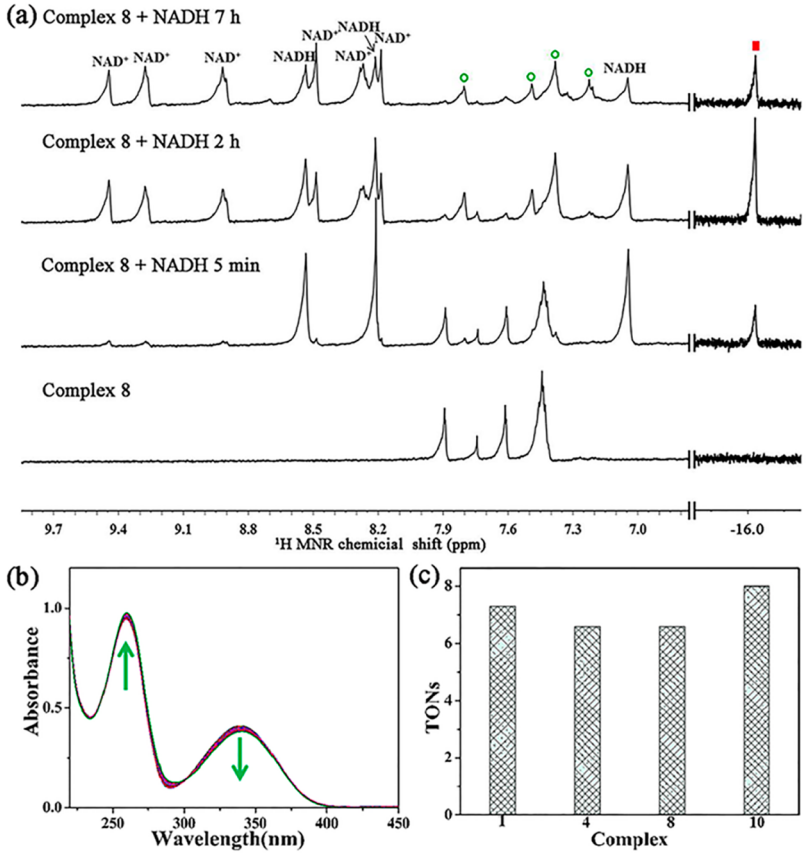

Figure 4. (a) ^{1}H NMR spectra of the reaction between complex $[(\eta^5\text{-}C_5Me_5)Ir(L8)Cl]PF_6^-$ (**8**) (1 mM) and NADH (3.5 mol equiv) in 50% CD_3OD-d_4/50% D_2O (v/v) at 310 K after 5 min, 2 h, and 7 h. Left: Low-field region. Right: High-field region showing the Ir−H hydride peak (−16.05 ppm). Peaks labeled with a green circle and red box correspond to the formed Ir−H complex. (b) UV−vis spectra of the reaction of NADH (100 μM) with complex $[(\eta^5\text{-}C_5Me_5)Ir(L8)Cl]PF_6^-$ (**8**) (1 μM) in 5% MeOH/95% H_2O (v/v)at 298 K for 8 h. (c) The turnover numbers (TONs) of complexes **1**, **4**, **8**, and **10**.

vitro anticancer activity significantly superior to complexes **1** (>100 μM), **2** (>100 μM), **3** (25.86 μM), and **4** (14.05 μM) containing the same substituents (R_1 and R_2) against A549 cancer cell lines. In addition, when ortho-substituents in the aniline is changed into the hydrogen atom, complex **11** becomes inactive (>100 μM). Next, maintaining the aniline ring substituent unchanged and increasing tether length on the imidazole ring gradually, the cytotoxicity follows the order of butyl- > isopropyl- > ethyl- > methyl-substituted NHCs. As a result, the tether length perturbations also exhibit variation on the anticancer activities of these complexes.

Pervious work has shown that the anticancer activity of half-sandwich iridium(III) complexes containing classical bipyridine chelating ligands increases by the incorporation of phenyl substituents on Cp*.[11] In this work, the introduction of biphenyl substituents onto the tetramethylcyclopentadienyl ring to obtain the complex $[(\eta^5\text{-}C_5Me_4C_6H_4C_6H_5)Ir(L1)Cl]PF_6^-$ (**12**) (IC_{50} = 7.44 μM) also results in enhanced cytotoxicity as compared to its parent Cp* complex $[(\eta^5\text{-}C_5Me_5)Ir(L1)Cl]PF_6^-$ (**1**) (IC_{50} > 100 μM). Finally, the influence of the substituent on the imine carbon on anticancer activity of these complexes was further investigated. Replacement of the methyl group on the imine carbon by a more electron-poor phenyl ring leads to complexes **9** (IC_{50} = 3.94 μM) and **10** (IC_{50} = 3.64 μM), which display approximately 6.6 and 3.9 times higher anticancer efficacy than complexes **3** (IC_{50} = 25.86 μM) and **10** (IC_{50} = 14.05 μM) against A549 cells lines, respectively. This result suggests that anticancer activity of these complexes could be tuned through electronic changes of the substituents on the imine carbon.

In this system, minor structural changes on four positions of the complex have a pronounced effect on their biological behaviors. As a result, this class of iridium(III) complexes represents a versatile and potent platform for development of organometallic anticancer metal containing drugs.

Reaction with NADH. In a sea of biocatalyzed processes, the coenzyme NADH and NAD^+ are a significant redox pair. Previous work has shown that half-sandwich iridium(III) anticancer complexes can accept a hydride from NADH and promote the production of ROS H_2O_2, thus providing a pathway to an oxidant mechanism of action.[12] Reactions between the iridium(III) complexes and NADH in 50% CD_3OD-d_4/50% D_2O (v/v) were monitored by ^{1}H NMR spectroscopy (complex **1**, Figure S34; complex **8**, Figure 4a).

When NADH (3.5 mol equiv) was added to a 1 mM solution of complex **8**, NADH was converted into its oxidized form NAD^+. A new set of low-field peaks at 8.92, 9.28, and 9.44 ppm assignable to the protons at the C4, C6, and C2 positions of the nicotinamide ring of NAD^+ and a sharp singlet at −16.05 ppm corresponding to the Ir^{III} hydride complex $[(\eta^5\text{-}Cp^*)Ir(L8)H]PF_6^-$ (Figure 4a) were observed after 5 min. The reaction of complex **1** with NADH also had the similar results (Figure S34). In a solution of complex **8** (0.5 mM) with NADH (3 mol equiv) in 50% MeOH/50% H_2O (v/

DOI: 10.1021/acs.inorgchem.8b01656
Inorg. Chem. XXXX, XXX, XXX−XXX

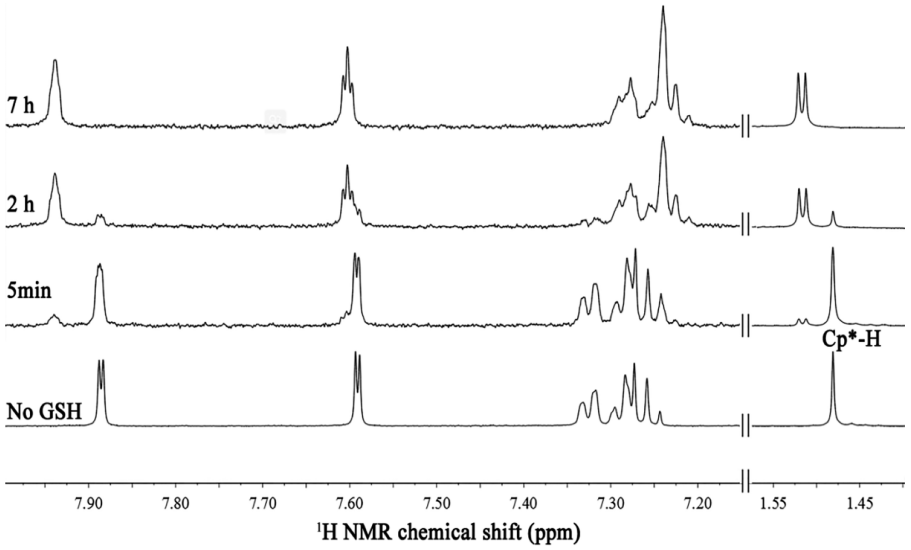

Figure 5. Dependence on time of the interaction of complex **4** (1 mM in CD_3OD-d_4/D_2O (1/1 v/v)) with GSH (25 mM, in D_2O, pH* adjusted to 7.2 ± 0.1), monitored by ^1H NMR (500 MHz) at 310 K.

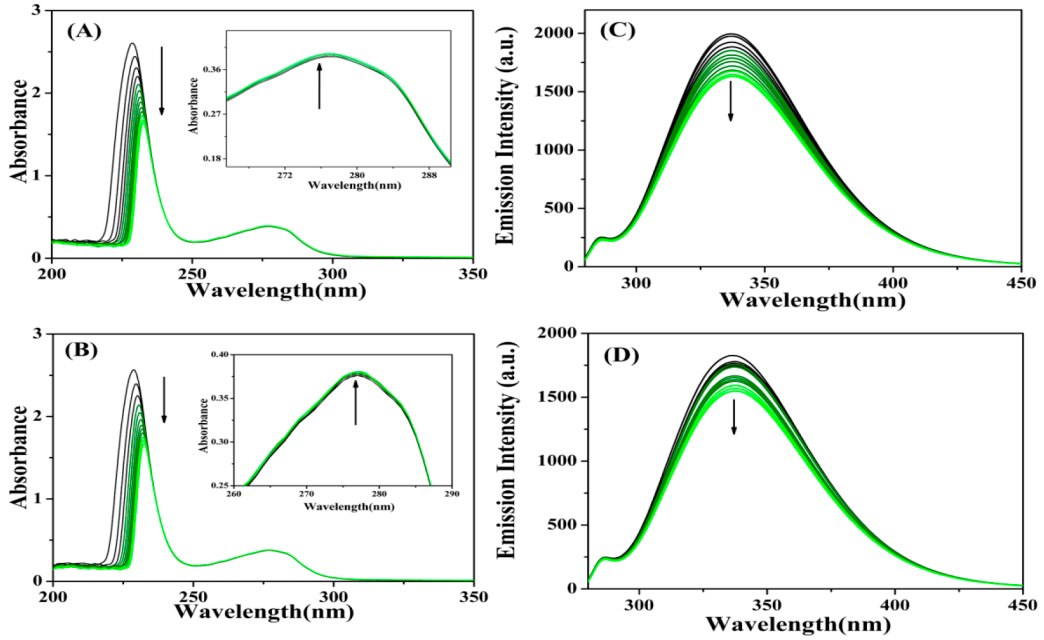

Figure 6. UV−vis spectrum of BSA (10 μM) in 5 mM Tris-HCl/10 mM NaCl buffer solution (pH 7.2) upon addition of the complex **4** (A) or **8** (B) (0−10 μM). Inset: Wavelength from 260 to 290 nm. Fluorescence spectra of BSA (10 μM; λ_{ex} = 280 nm; λ_{em} = 343 nm) in the absence and presence of the complex **4** (C) or **8** (D) (0−10 μM). The arrow shows the intensity changes in increasing concentration of the iridium(III) complex.

v) at 298 K, the ROS hydrogen peroxide was detected by the appearance of a blue color on hydrogen peroxide-test paper. In order to investigate the effect of four positions bearing different substituents in this complex framework on the catalytic ability, the reactions of complexes **1**, **4**, **8**, and **10** (~1 μM) with NADH (100 μM) in 5% MeOH/95% H_2O (v/v) were also investigated by UV−vis at 298 K (Figures 4b and S35). The turnover numbers (TONs) of complexes **1** (7.3), **4** (6.6), **8** (6.6), and **10** (8.0) were calculated by detecting the changes in absorbance at 339 nm (Figure 4c). These results suggest that the steric hindrance of ortho-substituents on the aniline moiety, the length of the alkyl substitutions on the imidazole ring and the electronic perturbations on the imine carbon appear to exhibit little variation on the catalytic activity of these complexes.

Interaction with Nucleobases. Reactions of complexes **4** and **8** with model nucleobase 9-ethylguanine (9-EtG) or 9-methyladenine (9-MeA) were monitored using the ^1H NMR spectroscopy from 5 min to 24 h. Solutions of **4** and **8** (~1 mM) and 2.0 molar equiv of 9-EtG or 9-MeA in 50% CD_3OD-d_4/50% D_2O (v/v) were prepared, respectively, and ^1H NMR spectra were recorded at different time intervals at 310 K. The NMR data do not show additional ^1H NMR peaks over a period of 24 h (Figures S36−S39), suggesting that no reaction with model nucleobase occurred for complexes **4** and **8**. Also, the formation of nucleobase adducts was not detected by mass

DOI: 10.1021/acs.inorgchem.8b01656
Inorg. Chem. XXXX, XXX, XXX−XXX

Table 2. Quenching Parameters and Binding Parameters for the Interaction of the Complexes 4 and 8 with BSA

complex	T (K)	K_{sv} (10^4)	K_q ($\times 10^{12}$ M^{-1} S^{-1})	K_b ($\times 10^4$ M^{-1})	n
4	298	2.68 ± 0.28	2.68	1.73	1.181
8	298	3.66 ± 0.15	3.66	12.8	0.304

spectrometry. So DNA may not be the main target for this type of iridium(III) complexes.

Reaction with GSH. Glutathione (GSH), the most plentiful nonprotein molecule in the cell, is involved in the detoxification of a lot anticancer agents.[13] Previous work has shown that GSH can reaction with iridium(III) and ruthenium(II) complexes through the coordination of thiol group to metal center.[14] The time dependence of the reaction of complexes **4** and **8** with tripeptide glutathione (GSH) were monitored by ^{1}H NMR under the same conditions: complex **4** or **8** (1 mM) in CD_3OD-d_4/D_2O (1/1 v/v, pH* adjusted to 7.2 ± 0.1) with GSH (25 mM) tested by ^{1}H NMR spectroscopy from 5 min to 7 h at 310 K. As shown in Figures 5 and S40, the low-field ligand-phenyl and imidazole ring peaks of Ir−Cl complex decreased gradually, and a new set of low-field resonances appeared when the excess GSH (25 mol equiv) was added. After 7 h, the Ir-Cl complex has been converted into the glutathione adducts (Ir−SG) completely. On the other hand, the five methyl groups in the Cp* ring of complexes **4** and **8** give rise to one singlet, but split into one doublet with an intensity ratio of 1:1 for Ir-SG. Complexes **4** and **8**, which contain an unsymmetric chelating ligand, are chiral. Thus, two diastereomeric glutathione adducts are expected.[14b] These results suggest that complexes **4** and **8** can reaction with GSH and Ir-SG adduct formed rapidly. This high glutathione affinity may mean that these iridium(III) complexes bind rapidly to GSH on entering cells. Thus, the binding of these iridium(III) complexes to DNA was blocked. This may explain why DNA is not a major target in this system.

Protein Binding Studies. The reactions of metal-base anticancer agents with proteins have attracted much attention since these interactions might feature processes that are significant for the toxicity, the biodistribution, and even the mechanism of action of anticancer agents.[15] Serum albumin, which possesses significant binding properties and highest content in blood plasma, plays an essential role in the drug transport system.[16] In this work, BSA (bovine serum albumin), owing to its structural similarity with human serum albumin (HSA), is chosen to study the binding of complexes to serum albumin.

The UV−vis absorption spectra of BSA were measured before and after the addition of complexes **4** and **8**. The results are shown in Figure 6, A and B. Upon addition of the complexes, the absorption peak at 228 nm decreased dramatically and shifted toward longer wavelength. The decrease of absorbance is due to the induced perturbation of the α-helix of BSA by the transition metal-based complexes.[17] The obvious red-shift in the absorption spectra is associated with the polarity of their surroundings. With the addition of iridium(III) complexes to BSA, a progressive increase without any shift was found in the absorption peak of BSA at 278 nm for these complexes, suggesting that the anticancer metallodrugs can interact with the BSA molecule and the microenvironments of the three aromatic acid residues in BSA (Trp, Tyr, and Phe) are altered.

Quenching of the emission intensity of BSA has been performed in the presence of the complexes to further understand the nature of binding complexes with BSA. In this work, the fluorescence measured was calibrated to correct the "inner filter" effect.[18] As shown in Figure 6, C and D, the fluorescence intensity of BSA at ~343 nm gradually decreased with the increase of concentration of complexes, suggesting that the complexes **4** and **8** can interact with BSA through static quenching mode. The possible quenching mechanism can be interpreted using the Stern−Volmer equation (eq 1)[19]

$$F_0/F = 1 + K_{sv}[Q] = 1 + K_q\tau_0[Q] \quad (1)$$

where F_0 and F are the steady-state fluorescence intensities in the absence and presence of the quenching agent, respectively, [Q] represents the total concentration of the quenching agent, K_q is the quenching rate constant, and τ_0 is the average lifetime of protein in the absence of quencher, and its value is 10^{-8} s.[20] K_{sv} is Stern−Volmer quenching constant which can be obtained from the ratio of the slope to the intercept of the plot of F_0/F versus the concentration of the tested complex (Figure S41). The corresponding Stern−Volmer quenching constants K_{sv} and quenching rate constants k_q are given in Table 2.

The calculated value of K_q for the complexes **4** and **8** are 2.68×10^{12} M^{-1} s^{-1} and 3.66×10^{12} M^{-1} s^{-1}, respectively, which are about 2 orders of magnitude higher than that of purely dynamic quenching mechanism (2.0×10^{10} M^{-1} s^{-1}).[21] The value of K_q indicates that a static quenching mechanism dominates in the interaction between iridium(III) complexes and BSA. The binding constant K_b and number of complex bound to BSA (n) are calculated (Figure S42), using the following formula (eq 2):[22]

$$\log[(F_0 - F)/F] = \log K_b + n \log[Q] \quad (2)$$

By comparison of the values of K_q and K_b, it is inferred that complex **8** interacts with BSA more strongly than the complex **4**. Thus, when the bulkiness of ortho-substituents in the aniline increases, the binding constant value (K) also increases. The difference of this binding ability between complexes **4** and **8** may cause differences in the anticancer activity of these complexes.

Synchronous fluorescence spectrometry is a very useful technique for obtaining information about molecular environment in the vicinity of the fluorophore molecules at low concentrations under analogous conditions.[23] The use of $\Delta\lambda$ = 15 nm and $\Delta\lambda$ = 60 nm gives the spectral property of tyrosine residues and tryptophan residues, respectively.[24] It can be seen from Figure S43, that the synchronous fluorescence intensity for BSA with increasing concentrations of complex **4** displayed a decrease at 292 nm ($\Delta\lambda$ = 15 nm) with an inappreciable blue shift of 1 or 2 nm. At the same time, the emission wavelength of tryptophan residues did not undergo significant changes during the binding process. These results indicated that the reaction of complexes with BSA can influence the conformation of the tyrosine microregion. In addition, the slight blue shift is mainly due to the fact that the active site in protein is buried in a hydrophobic environment.[25] Therefore, the hydrophobicity around tyrosine residues is reinforced in this system. The valid binding of the complex with the BSA was

DOI: 10.1021/acs.inorgchem.8b01656
Inorg. Chem. XXXX, XXX, XXX−XXX

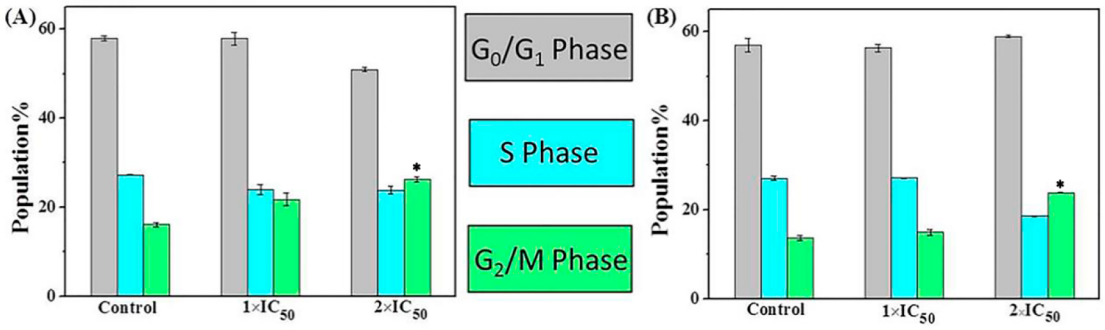

Figure 7. Flow cytometry data for cell cycle distribution of A549 cancer cells exposed to complexes **4** (A) and **8** (B) for 24 h. Concentrations used were 1 and 2 equipotent concentrations of IC_{50}. Cell staining for flow cytometry was carried out using PI/RNase. Data are quoted as mean ± SD of three replicates. *P*-Values were calculated after a *t* test against the negative control data, $*p < 0.05$.

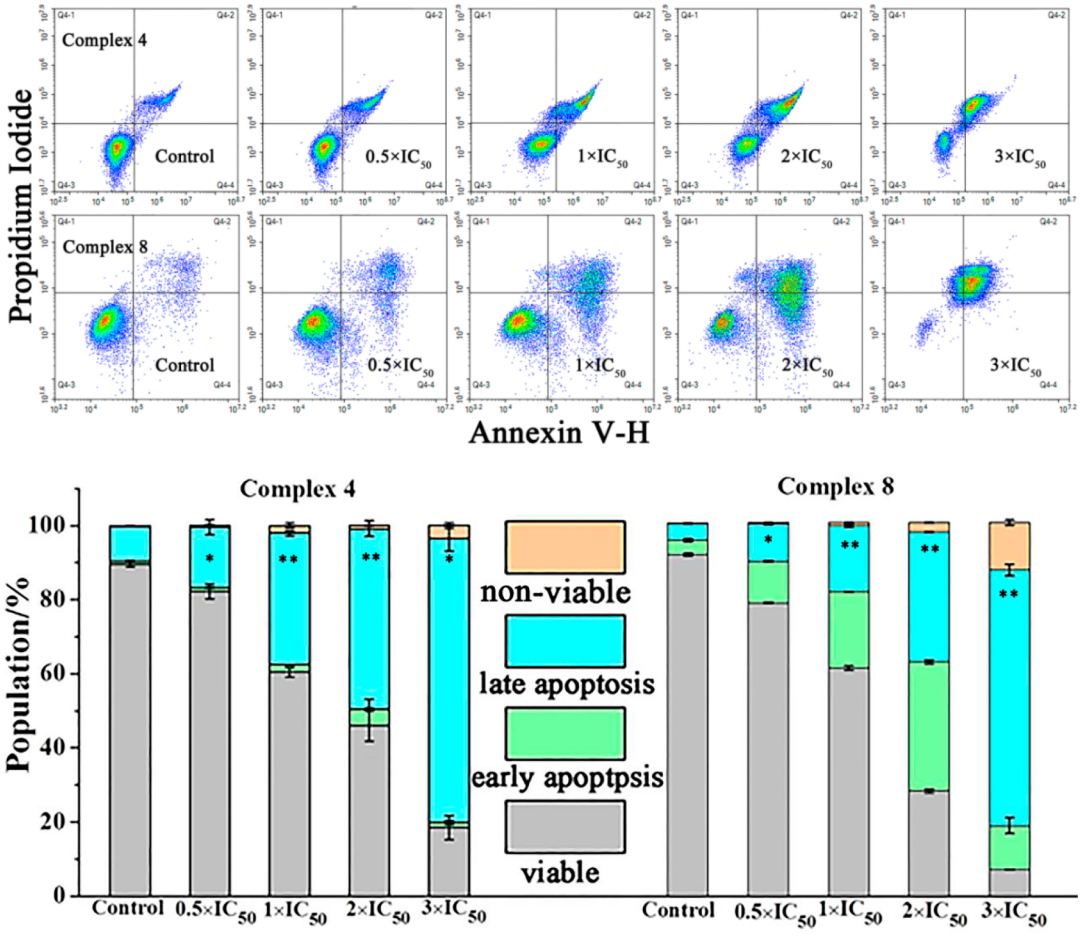

Figure 8. Apoptosis analysis of A549 cells after 24 h of exposure to complexes **4** and **8** at 310 K determined by flow cytometry using annexin V-FITC vs PI staining. Populations for cells in four stages treated by complexes **4** and **8**. Data are quoted as mean ± SD of three replicates. *p*-Values were calculated after a *t* test against the negative control data, $*p < 0.05$ and $**p < 0.01$.

confirmed via the hydrophobicity observed in fluorescence and synchronous experiments. Hence, the strong interaction of these complexes with BSA suggested that BSA can be considered as an excellent carrier for delivery of anticancer agents in vivo.

Cell Cycle Arrest. Generally, most anticancer metallodrugs exert their anticancer efficacy via genomic DNA damage and cell cycle perturbation.[26] To understand the impact of the new complexes on cell growth, complexes **4** and **8** effect on the cell cycle by flow cytometry analysis in A549 cancer cells was evaluated. A549 cells were treated with different concentrations ($1 \times IC_{50}$ and $2 \times IC_{50}$) of complexes **4** and **8** for 24 h (Figures 7 and S44 and Tables S4–S5), respectively. In comparison to negative control populations, both complexes **4** and **8** arouse an increased 10.2% of cells in the G_2/M phase at a concentration of $2 \times IC_{50}$, suggesting that complexes **4** and **8** arrest the cell cycle at the G_2/M phase in a concentration-dependent manner.

Apoptosis Assay. To quantify the amount of cells in different apoptosis stages, A549 cells were treated with complexes **4** and **8** at 0.5, 1, 2, and 3 equipotent concentrations of IC_{50} for 24 h, and then analyzed by flow cytometry. The

DOI: 10.1021/acs.inorgchem.8b01656
Inorg. Chem. XXXX, XXX, XXX−XXX

results are shown in Figure 8 and Tables S6–S7. When complexes **4** and **8** is at 3 equipotent concentrations of IC_{50}, a total of 78.1% and 80.1% of cells were undergoing apoptosis, respectively. As shown in the histogram (Figure 8), the most apoptotic cells are in late apoptosis stage. This indicated that cell death can be induced through a high incidence of apoptosis. In addition, complex **8** showed slightly enhanced ability to induce apoptosis of A549 cells, which is consistent with its higher anticancer activity compared to complex **4**.

ROS Determination. Mitochondria are the main sites of cellular ROS production, and mitochondrial dysfunction may lead to ROS accumulation during the process of apoptosis.[27] The levels of ROS in A549 cells were estimated by flow cytometry analysis. Treatment of A549 cells with complex **8** for 24 h results in a dose-dependent increase in the production of ROS (Figure 9). This result indicates that complex **8** may lead to ROS accumulation. Elevated levels of reactive oxygen species may be responsible for the cell toxicity of these complexes.

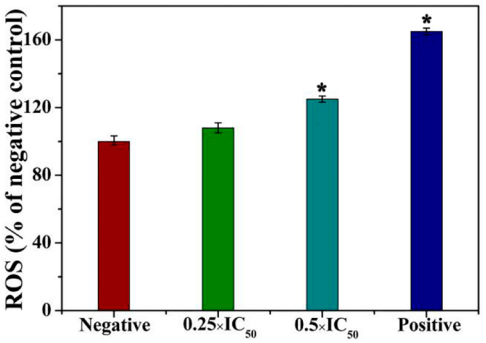

Figure 9. Analysis of ROS levels by flow cytometry after A549 cells were treated with complex **8** at the 0.25 and 0.5 equipotent concentrations of IC_{50} for 24 h and stained with H_2DCFDA. *p*-Values were calculated after a *t* test against the negative control data, $*p < 0.05$.

Impact on Mitochondrial Membrane Potential (MMP). Mitochondrial plays a central role in apoptosis because they can generate a large of the ATP in cells. The decrease of mitochondrial membrane potential is an important indicator for the detection of apoptosis. The effects of complexes **4** and **8** on MMP were determined by 5,5′,6,6′-tetrachloro-1,1′,3,3′-tetraethylbenzimidazolylcarbocyanine iodide (JC-1) using flow cytometry. As shown in Figure 10 and Tables S8–S9, increasing the concentration of complexes **4** and **8** result in an obvious red-to-green color shift, which marks the loss of MMP. The percentage of cells with mitochondrial membrane depolarization increases from 10.72% to 61.15% and 7.67% to 50.10% for **4** and **8** at a concentration of $2 \times IC_{50}$, respectively. Additionally, as shown in Figure S45 and Table S10, the JC-1 red/green fluorescence ratios reduced from 8.34 ± 0.42 to 0.64 ± 0.01 and 12.14 ± 1.67 to 1.00 ± 0.04 for **4** and **8** at a concentration of $2 \times IC_{50}$, respectively. As a result, the dysfunction of MMP may contribute to the anticancer activity of these iridium(III) complexes.

Cellular Localization. Because of luminescence properties of these iridium(III) complexes, we subsequently examined the cellular localization of these complexes using confocal microscopy. Organelle-specific probes are powerful tools that can real-time monitor morphological changes of organelle and intracellular dynamic processes.[28] To evaluate which organelles would be targeted by these iridium(III) complexes, the A549 cells were dual-stained with complex **8** and different organelle-specific probes, respectively. Confocal microscopic imaging indicates that the complex **8** can effectively enter A549 cells after 1 h incubation, as indicated by the intense and punctate green fluorescence in the cytoplasm (Figure 11). Co-localization analysis with the organelle-specific stain for lysosome shows excellent concordance between overlay images of the complex **8** (10 μM) and conventional LTDR (75 nM) in A549 cells. Pearson's correlation coefficients for complex **8** and LTDR is 82%. Clearly, complex **8** is selectively localized within lysosome and the cytotoxic properties may originate from lysosome mediated cell death.

Lysosomal Damage. The dysfunction of lysosomes of A549 cells was evaluated via acridine orange (AO) staining. AO is a useful probe employed to assess the lysosomal functional state at subcellular level, because it emits a concentration-dependent red/green fluorescence.[29] As shown in Figure 12, A549 cells treated with only acridine orange(AO) (5 μM) showed distinct red fluorescence in lysosomes, suggesting that lysosomes under such conditions were intact. However, the red fluorescence of AO significantly decreased with the increase of drug concentration, which suggested that lysosomal integrity was jeopardized upon complex **8** treatments. These results indicated that complex **8** can induce apoptosis through lysosomal damage.

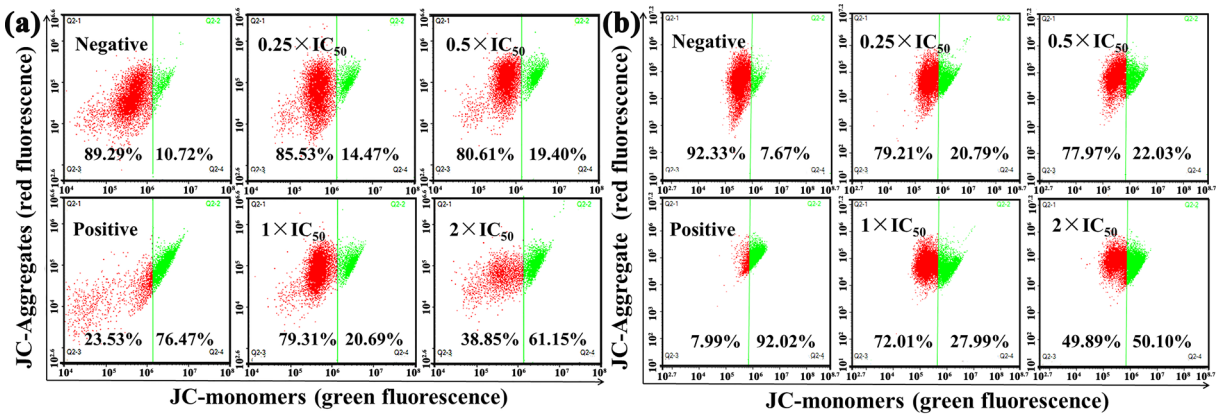

Figure 10. Changes in mitochondrial membrane potential of A549 cancer cells induced by complexes **4** (a) and **8** (b).

DOI: 10.1021/acs.inorgchem.8b01656
Inorg. Chem. XXXX, XXX, XXX–XXX

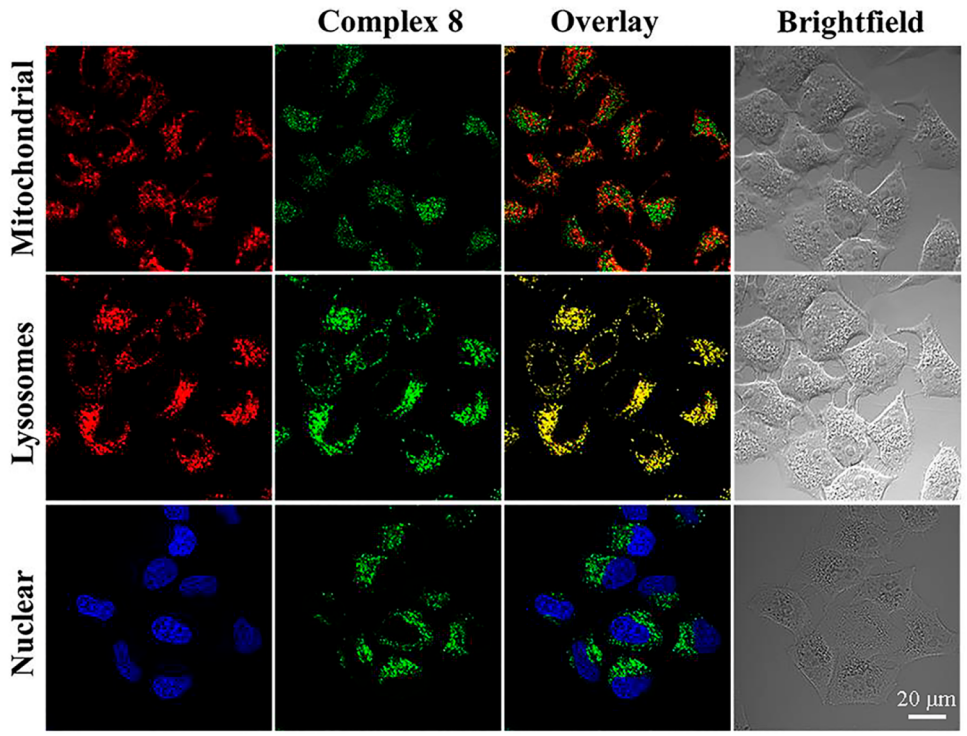

Figure 11. Determination of intercellular localization of complex **8** by confocal microscopy. A549 cells were incubated with complex **8** (10 μM) for 1 h at 37 °C, then coincubated with MTDR (500 nM), LTDR (75 nM) and DAPI (1 μg/mL) for 20 min, respectively. Complex **8** was excited at 488 nm and the emission was collected at 520 ± 20 nm. MTDR was excited at 543 nm and the emission was collected at 690 ± 30 nm; LTDR was excited at 594 nm and the emission was collected at 630 ± 30 nm. DAPI was excited at 405 nm and the emission was collected at 460 ± 30 nm. Scale bar: 20 μm.

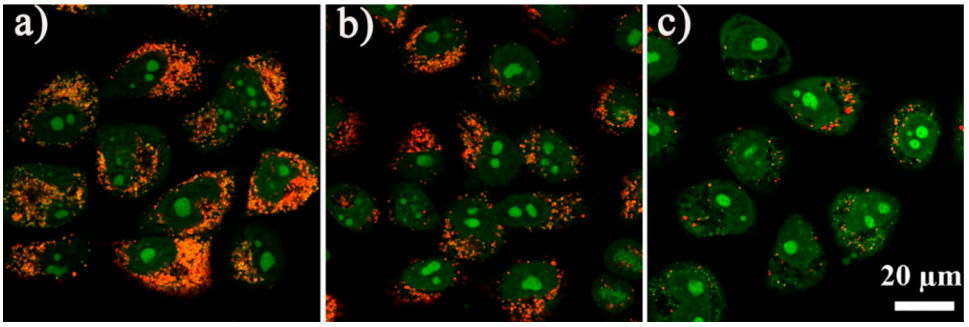

Figure 12. Observation of lysosomal disruption in A549 cells loaded with complex **8** for 6 h at 37 °C, then stained with acridine orange (AO) (5 μM) at 37 °C for 15 min. Emission was collected at 510 ± 20 nm (green) and 625 ± 20 nm (red) upon excitation at 488 nm. Scale bar: 20 μm. The A549 cells were treated with (a) only acridine orange (AO); (b) acridine orange (AO) and complex **8** (1× IC_{50}); (c) acridine orange (AO) and complex **8** (3× IC_{50}).

Cellular Uptake Mechanisms. We also further investigated the cellular uptake mechanisms of complex **8** in A549 cells. The ways in which small molecules enter cells include energy-dependent or energy-independent pathways.[30] As shown in Figure 13, A549 cells incubated with complex **8** at 4 °C or pretreated with carbonyl cyanide *m*-chlorophenyl hydrazone (CCCP) resulted in a reduced intracellular luminescence intensity compared to untreated control group (37 °C). However, intracellular luminescence intensity was not significantly influenced by the endocytosis inhibitor chloroquine. These results suggest that the cellular uptake of complex **8** is mainly through a well-known energy-dependent mechanism, such as active transport. Endocytosis was not responsible for the uptake of complex **8**.

Observation of Nuclear Morphology. The investigation of nuclear morphology of the A549 cells was also performed by confocal microscopy using nucleus-staining dye 4′,6-diamidino-2-phenylindole (DAPI). Confocal microscopic images are shown in Figure S46. As time goes on, the volume of nucleus gradually decreases and the surface of the nucleus becomes nonsmooth. In addition, nuclear condensation occurs, and then the nucleus is broken into fragments of different sizes. Further, the presence of apoptotic bodies was also detected. These results suggested that complex **8** can change nuclear morphology effectively and finally induce cells apoptosis.

Antibacterial Studies. To further investigate the potentiality of such complexes as antibacterial agents, complexes **4** and **8** were chosen and preliminary studied against two bacterial strains, the Gram-positive *Staphylococcus*

DOI: 10.1021/acs.inorgchem.8b01656
Inorg. Chem. XXXX, XXX, XXX−XXX

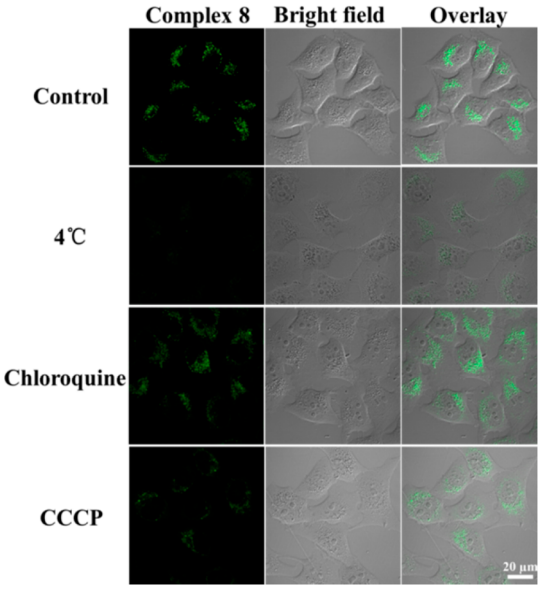

Figure 13. Confocal images of A549 cells after incubation with complex **8** (10 μM) under different conditions. (A) Cells were incubated with complex **8** (10 μM) at 37 °C for 1 h. (B) Cells were incubated with complex **8** (10 μM) at 4 °C for 1 h. (C) Cells were preincubated with CCCP (50 μM) for 1 h at 37 °C and then incubated with complex **8** (10 μM) at 37 °C for 1 h. (D) Cells were preincubated with chloroquine (50 μM) for 1 h at 37 °C and then incubated with complex **8** (10 μM) at 37 °C for 1 h. Complex **8** was excited at 488 nm and emission was collected at 520 ± 20 nm. Scale bar: 20 μm.

aureus (*S. aureus*) and the Gram-negative *Proteus vulgaris* (*P. vulgaris*). As illustrated in Figure 14, the *S. aureus* and *P.*

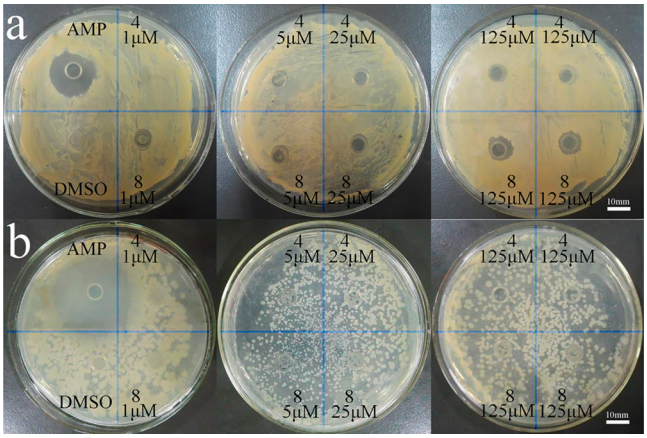

Figure 14. Antibacterial activity of complexes **4** and **8** (1, 5, 25, and 125 μM) were determined by the Oxford Cup method. (a) The anti-*S. aureus* activity of complexes **4** and **8**. (b) The anti-*P. vulgaris* activity of complexes **4** and **8**. Ampicillin (AMP) was used as the positive control (100 μg mL^{-1}). Scale bar: 10 mm.

vulgaris diameter of inhibition zone are 19 mm and 33 mm, respectively. Interestingly, an obviously inhibition zone was observed when the *S. aureus* was treated with maximum concentration of complex **8** (the diameter of inhibition zone is 11 mm), and no inhibition zone was observed when the *S. aureus* was treated with the same concentration of complex **4** (Figure 14a), suggesting that complex **8** exhibited higher efficiency than complex **4** in the growth inhibition of *S. aureus*. This result is consistent with their cytotoxicity. Additionally, as shown in Figure 14b, complexes **4** and **8** showed no activity against *P. vulgaris*. It seems that complex **8** exhibited selective antibacterial activity toward *S. aureus*.

CONCLUSIONS

To conclude, a series of novel and versatile imine-N-heterocyclic carbene-based half-sandwich iridium(III) anticancer complexes of the type $[(\eta^5\text{-Cp}^x)\text{Ir(C^N)Cl}]\text{PF}_6^-$ have been designed and prepared. Spectroscopic properties study displays that complex **8** has a detectable fluorescence. This type of imine-N-heterocyclic carbene half-sandwich iridium(III) complex appears to be the first time used as anticancer agents. In this complex framework, substituents on four positions could be modulated, which provides a large amount of flexibility and opportunities to tune the cytotoxicity of complexes. The structure−activity relationships are very significant. With increasing the size of the substituents on aniline moiety and imidazole ring, the anticancer activity increased. In addition, the complexes containing the electron-poor groups seem to have the higher anticancer activity than that containing the electron-rich groups.

No nucleobase binding was observed for these complexes, indicating that DNA is not a possible target. This type of complexes can react with GSH and catalyze oxidation of NADH to NAD^+. Further, they showed moderate binding affinity to BSA and the fluorescence quenching of BSA by the metal complexes is due to the static quenching. As a result, binding of complexes **4** and **8** with BSA can reach the designated target through blood transport. Additionally, the complexes **4** and **8** aroused a decrease in mitochondrial membrane potential, disturbed the cell cycle at G_2/M phase and induced obvious cell apoptosis in A549 cancer cells. Complex **8** can also induce high increase in the level of ROS in A549 cancer cells. It seems that cell cycle, apoptosis induction, ROS level and mitochondrial membrane potential together contribute to the anticancer potency of these iridium(III) complexes.

Confocal imaging studies indicated that the typical and most active complex **8** entered A549 lung cancer cells mainly through energy-dependent pathway and was located in lysosome. The cytotoxic properties may originate from lysosome mediated cell death. Furthermore, lysosomal damage and nuclear morphology were detected in A549 cancer cells by confocal microscopy. Nuclear condensation and apoptotic bodies may finally induce cells apoptosis. Interestingly, complex **8** also showed antibacterial activity against Gram-positive *S. aureus*. All of these preliminary results suggest that this type of iridium(III) complexes containing versatile imine-N-heterocyclic carbene ligands could be a promising candidate for future cancer therapy.

ASSOCIATED CONTENT

Supporting Information

The Supporting Information is available free of charge on the ACS Publications website at DOI: 10.1021/acs.inorgchem.8b01656.

Details of the experimental section, Figures S1−S46, and Tables S1−S10 (PDF)

Accession Codes

CCDC 1843724 and 1843726 contain the supplementary crystallographic data for this paper. These data can be obtained

DOI: 10.1021/acs.inorgchem.8b01656
Inorg. Chem. XXXX, XXX, XXX−XXX

free of charge via www.ccdc.cam.ac.uk/data_request/cif, or by emailing data_request@ccdc.cam.ac.uk, or by contacting The Cambridge Crystallographic Data Centre, 12 Union Road, Cambridge CB2 1EZ, UK; fax: +44 1223 336033.

AUTHOR INFORMATION

Corresponding Authors

*E-mail: guolihua@qfnu.edu.cn.
*E-mail: liuzheqd@163.com.

ORCID

Lihua Guo: 0000-0002-0842-9958
Zhe Liu: 0000-0001-5796-4335

Notes

The authors declare no competing financial interest.

ACKNOWLEDGMENTS

We thank Shandong Provincial Natural Science Foundation (ZR2018MB023), the National Natural Science Foundation of China (Grant No. 21671118), the Taishan Scholars Program, the Key Laboratory of Polymeric Composite & Functional Materials of Ministry of Education (PCFM-2017-01), and the excellent experiment project of Qufu Normal University (jp201705) for support.

REFERENCES

(1) (a) Bourissou, D.; Guerret, O.; Gabbaï, F. P.; Bertrand, G. Stable carbenes. *Chem. Rev.* **2000**, *100*, 39−92. (b) Herrmann, W. A. N-Heterocyclic Carbenes: A New Concept in Organometallic Catalysis. *Angew. Chem., Int. Ed.* **2002**, *41*, 1290−1309. (c) Crudden, C. M.; Allen, D. P. Stability and reactivity of N-heterocyclic carbene complexes. *Coord. Chem. Rev.* **2004**, *248*, 2247−2273. (d) Guo, L. H.; Kong, W. Y.; Xu, Y. J.; Yang, Y. L.; Ma, R.; Cong, L.; Dai, S. Y.; Liu, Z. Large-scale synthesis of novel sterically hindered acenaphthene-based α-diimine ligands and their application in coordination chemistry. *J. Organomet. Chem.* **2018**, *859*, 58−67. (e) Lee, H. M.; Lee, C. C.; Cheng, P. Y. Recent Development of Functionalized N-heterocyclic Carbene Ligands: Coordination Chemistry and Catalytic Applications. *Curr. Org. Chem.* **2007**, *11*, 1491−1524. (f) Kühl, O. The chemistry of functionalised N-heterocyclic carbenes. *Chem. Soc. Rev.* **2007**, *36*, 592−607. (g) Hahn, F. E.; Jahnke, M. C. Heterocyclic Carbenes: Synthesis and Coordination Chemistry. *Angew. Chem., Int. Ed.* **2008**, *47*, 3122−3172. (h) Díez-González, S.; Marion, N.; Nolan, S. P. N-Heterocyclic Carbenes in Late Transition Metal Catalysis. *Chem. Rev.* **2009**, *109*, 3612−3676.

(2) Xiong, S. Y.; Guo, L. H.; Zhang, S. M.; Liu, Z. Asymmetric Cationic [P, O] Type Palladium Complexes in Olefin Homopolymerization and Copolymerization. *Chin. J. Chem.* **2017**, *35*, 1209−1221.

(3) (a) Herrmann, W. A. N-heterocyclic carbenes: a new concept in organometallic catalysis. *Angew. Chem., Int. Ed.* **2002**, *41*, 1290−1309. (b) Guo, L. H.; Liu, W. J.; Chen, C. L. Late transition metal catalyzed α-olefin polymerization and copolymerization with polar monomers. *Mater. Chem. Front.* **2017**, *1*, 2487−2494. (c) Li, Y.; Tan, C. P.; Zhang, W.; He, L.; Ji, L. N.; Mao, Z. W. Phosphorescent iridium(III)-bis-N-heterocyclic carbene complexes as mitochondria-targeted theranostic and photodynamic anticancer agents. *Biomaterials* **2015**, *39*, 95−104. (d) Guo, L. H.; Dai, S. Y.; Sui, X. L.; Chen, C. L. Palladium and nickel catalyzed chain walking olefin polymerization and copolymerization. *ACS Catal.* **2016**, *6*, 428−441. (e) Li, Y.; Liu, B.; Lu, X. R.; Li, M. F.; Ji, L. N.; Mao, Z. W. Cyclometalated iridium(III) N-heterocyclic carbine complexes as potential mitochondrial anticancer and photodynamic agents. *Dalton Trans.* **2017**, *46*, 11363−11371. (f) Guo, L. H.; Chen, C. L. α-Diimine)palladium catalyzed ethylene polymerization and (*co*)polymerization with polar comonomers. *Sci. China: Chem.* **2015**, *58*, 1663−1673. (g) Muenzner, J. K.; Rehm, T.; Biersack, B.; Casini, A.; de Graaf, I. A. M.; Worawutputtapong, P.; Noor, A.; Kempe, R.; Brabec, V.; Kasparkova, J.; Schobert, R. Adjusting the DNA Interaction and Anticancer Activity of Pt(II) N−heterocyclic Carbene Complexes by Steric Shielding of the Trans Leaving Group. *J. Med. Chem.* **2015**, *58*, 6283−6292.

(4) (a) Coleman, K. S.; Chamberlayne, H. T.; Turberville, S.; Green, M. L. H.; Cowley, A. R. Silver(I) complex of a new imino-N-heterocyclic carbene and ligand transfer to palladium(II) and rhodium(I). *Dalton Trans.* **2003**, *14*, 2917−2922. (b) Bonnet, L. G.; Douthwaite, R. E.; Kariuki, B. M. Synthesis of New Chiral N-Heterocyclic Carbene-Imine Ligands and Their Application to an Asymmetric Allylic Alkylation Reaction. *Organometallics* **2003**, *22*, 4187−4189. (c) Frøseth, M.; Dhindsa, A.; Røise, H.; Tilset, M. Synthesis and characterization of palladium(II) complexes with a novel chelating iminocarbene ligand. *Dalton Trans.* **2003**, *23*, 4516−4524. (d) Steiner, G.; Kopacka, H.; Ongania, K. H.; Wurst, K.; Preishuber-Pflügl, P.; Bildstein, B. Heteroditopic Imino N-Heterocyclic Carbenes and Their Sulfur, Selenium, and Tungsten Tetracarbonyl Derivatives. *Eur. J. Inorg. Chem.* **2005**, *2005*, 1325−1333. (e) Frøseth, M.; Netland, K. A.; Törnroos, K. W.; Dhindsa, A.; Tilset, M. Synthesis and characterization of novel Pd(II) complexes with chelating and non-chelating heterocyclic iminocarbene ligands. *Dalton Trans.* **2005**, *249*, 1664−1674. (f) Frøseth, M.; Netland, K. A.; Rømming, C.; Tilset, M. Synthesis and characterization of novel Pd(II) and Pt(II) complexes with 5-ring chelating iminoylcarbene ligands. *J. Organomet. Chem.* **2005**, *690*, 6125−6132. (g) Coleman, K. S.; Dastgir, S.; Barnett, G.; Alvite, M. J. P.; Cowley, A. R.; Green, M. L. H. A nonenolizable imino-N-heterocyclic carbene ligand and corresponding silver(I) metal complex. *J. Organomet. Chem.* **2005**, *690*, 5591−5596.

(5) (a) Hartinger, C. G.; Dyson, P. J. Bioorganometallic chemistry-from teaching paradigms to medicinal applications. *Chem. Soc. Rev.* **2009**, *38*, 391−401. (b) Gasser, G.; Ott, I.; Metzler-Nolte, N. Organometallic Anticancer Compounds. *J. Med. Chem.* **2011**, *54*, 3−25. (c) Che, C. M.; Siu, F. M. Metal complexes in medicine with a focus on enzyme inhibition. *Curr. Opin. Chem. Biol.* **2010**, *14*, 255−261. (d) Barton, J. K.; Olmon, E. D.; Sontz, P. A. Metal complexes for DNA-mediated charge transport. *Coord. Chem. Rev.* **2011**, *255*, 619−634. (e) Ronconi, L.; Sadler, P. J. Using coordination chemistry to design new medicines. *Coord. Chem. Rev.* **2007**, *251*, 1633−1648. (f) Yang, Y. L.; Guo, L. H.; Tian, Z. Z.; Liu, X. C.; Gong, Y. T.; Zheng, H. M.; Ge, X. X.; Liu, Z. Imine-N-heterocyclic carbene as versatile ligands in ruthenium(II) p-cymene anticancer complexes: a structure-activity relationship study. *Chem. Asian J.* **2018**, DOI: 10.1002/asia.201801058. (g) Du, Q.; Guo, L. H.; Tian, M.; Ge, X. X.; Yang, Y. L.; Jian, X. Y.; Xu, Z. S.; Tian, Z. Z.; Liu, Z. Potent Half-Sandwich Iridium(III) and Ruthenium(II) Anticancer Complexes Containing a P^O-Chelated Ligand. *Organometallics* **2018**, DOI: 10.1021/acs.organomet.8b00402.

(6) Tian, M.; Li, J. J.; Zhang, S. M.; Guo, L. H.; He, X. D.; Kong, D. L.; Zhang, H. R.; Liu, Z. Half-sandwich ruthenium(II) complexes containing N^N-chelated imino-pyridyl ligands that are selectively toxicto cancer cells. *Chem. Commun.* **2017**, *53*, 12810−12813.

(7) (a) Wang, C. L.; Liu, J. F.; Tian, Z. Z.; Tian, M.; Tian, L. J.; Zhao, W. Q.; Liu, Z. Half-sandwich iridium N-heterocyclic carbine anticancer complexes. *Dalton Trans.* **2017**, *46*, 6870−6883. (b) Li, J. J.; Guo, L. H.; Tian, Z. Z.; Tian, M.; Zhang, S. M.; Xu, K.; Qian, Y. C.; Liu, Z. Novel half-sandwich iridium(III) imino-pyridyl complexes showing remarkable in vitro anticancer activity. *Dalton Trans.* **2017**, *46*, 15520−15534. (c) Movassaghi, S.; Singh, S.; Mansur, A.; Tong, K. K. H.; Hanif, M.; Holtkamp, H. U.; Söhnel, T.; Jamieson, S. M. F.; Hartinger, C. G. (Pyridin-2-yl)-NHC organoruthenium complexes: antiproliferative properties and reactivity toward biomolecules. *Organometallics* **2018**, *37*, 1575−1584.

(8) Gong, P. W.; Guo, L. H.; Pang, M. H.; Wang, D. D.; Sun, L.; Tian, Z. Z.; Li, J. J.; Zhang, Y. Y.; Liu, Z. Nano-sized paramagnetic and fluorescent fluorinated carbon fiber with high NIR absorbance for cancer chemo-photothermal therapy. *J. Mater. Chem. B* **2018**, *6*, 3068−3077. (b) Wang, F. X.; Chen, M. H.; Lin, Y. N.; Zhang, H.; Tan, C. P.; Ji, L. N.; Mao, Z. W. Dual Functions of Cyclometalated

DOI: 10.1021/acs.inorgchem.8b01656
Inorg. Chem. XXXX, XXX, XXX−XXX

Iridium(III) Complexes: Anti-Metastasis and Lysosome-Damaged Photodynamic Therapy. *ACS Appl. Mater. Interfaces* **2017**, *9*, 42471−42481. (c) Gong, P. W.; Ji, S. J.; Wang, J. Q.; Dai, D. J.; Wang, F.; Tian, M.; Zhang, L.; Guo, F. F.; Liu, Z. Fluorescence-switchable ultrasmall fluorinated graphene oxide with high near-infrared absorption for controlled and targeted drug delivery. *Chem. Eng. J.* **2018**, *348*, 438−446.

(9) (a) Lo, K. K. W. Luminescent rhenium(I) and iridium(III) polypyridine complexes as biological probes, imaging reagents, and photocytotoxic agents. *Acc. Chem. Res.* **2015**, *48*, 2985−2995. (b) Chen, M. H.; Wang, F. X.; Cao, J. J.; Tan, C. P.; Ji, L. N.; Mao, Z. W. Light-up mitophagy in live cells with dual-functional theranostic phosphorescent iridium(III) complexes. *ACS Appl. Mater. Interfaces* **2017**, *9*, 13304−13314. (c) Huang, H. Y.; Zhang, P. Y.; Yu, B. L.; Chen, Y.; Wang, J. Q.; Ji, L. N.; Chao, H. Targeting nucleus DNA with a cyclometalated dipyridophenazineruthenium(II) complex. *J. Med. Chem.* **2014**, *57*, 8971−8983. (d) Cao, J. J.; Tan, C. P.; Chen, M. H.; Wu, N.; Yao, D. Y.; Liu, X. G.; Ji, L. N.; Mao, Z. W. Targeting cancer cell metabolism with mitochondria-immobilized phosphorescent cyclometalated iridium(III) complexes. *Chem. Sci.* **2017**, *8*, 631−640.

(10) Mosmann, T. Rapid colorimetric assay for cellular growth and survival: Application to proliferation and cytotoxicity assays. *J. Immunol. Methods* **1983**, *65*, 55−63.

(11) Liu, Z.; Habtemariam, A.; Pizarro, A. M.; Clarkson, G. J.; Sadler, P. J. Organometallic iridium(III) cyclopentadienyl anticancer complexes containing C,N-chelating ligands. *Organometallics* **2011**, *30*, 4702−4710.

(12) (a) Liu, Z.; Romero-Canelón, I.; Qamar, B.; Hearn, J. M.; Habtemariam, A.; Barry, N. P. E.; Pizarro, A. M.; Clarkson, G. J.; Sadler, P. J. The Potent Oxidant Anticancer Activity of Organoiridium Catalysts. *Angew. Chem.* **2014**, *126*, 4022−4027. (b) Zhang, H. R.; Guo, L. H.; Tian, Z. Z.; Tian, M.; Zhang, S. M.; Xu, Z. S.; Gong, P. W.; Zheng, X. F.; Zhao, J.; Liu, Z. Significant effects of counteranions on the anticancer activity of iridium(III) complexes. *Chem. Commun.* **2018**, *54*, 4421−4424.

(13) Garai-Ibabe, G.; Saa, L.; Pavlov, V. Enzymatic Product-Mediated Stabilization of CdS Quantum Dots Produced In Situ: Application for Detection of Reduced Glutathione, NADPH, and Glutathione Reductase Activity. *Anal. Chem.* **2013**, *85*, 5542−5546.

(14) (a) Chen, F.; Romero-Canelón, I.; Soldevila-Barreda, J. J.; Song, J. I.; Coverdale, J. P. C.; Clarkson, G. J.; Kasparkova, J.; Habtemariam, A.; Wills, M.; Brabec, V.; Sadler, P. J. Transfer Hydrogenation and Antiproliferative Activity of Tethered Half-Sandwich Organoruthenium Catalysts. *Organometallics* **2018**, *37*, 1555−1566. (b) Liu, Z.; Romero-Canelón, I.; Qamar, B.; Hearn, J. M.; Habtemariam, A.; Barry, N. P. E.; Pizarro, A. M.; Clarkson, G. J.; Sadler, P. J. The Potent Oxidant Anticancer Activity of Organoiridium Catalysts. *Angew. Chem., Int. Ed.* **2014**, *53*, 3941−3946.

(15) Dömötör, O.; Hartinger, C. G.; Bytzek, A. K.; Kiss, T.; Keppler, B. K.; Enyedy, E. A. Characterization of the binding sites of the anticancer ruthenium(III) complexes KP1019 and KP1339 on human serum albumin via competition studies. *JBIC, J. Biol. Inorg. Chem.* **2013**, *18*, 9−17.

(16) Mukhopadhyay, S.; Gupta, R. K.; Paitandi, R. P.; Rana, N. K.; Sharma, G.; Koch, B.; Rana, L. K.; Hundal, M. S.; Pandey, D. S. Synthesis, Structure, DNA/Protein Binding, and Anticancer Activity of Some Half-Sandwich Cyclometalated Rh(III) and Ir(III) Complexes. *Organometallics* **2015**, *34*, 4491−4506.

(17) (a) Kang, J.; Liu, Y.; Xie, M. X.; Li, S.; Jiang, M.; Wang, Y. D. Interactions of human serum albumin with chlorogenic acid and feluric acid. *Biochim. Biophys. Acta, Gen. Subj.* **2004**, *1674*, 205−214. (b) Abou-Zied, O. K.; Al-Shihi, O. I. K. Characterization of subdomain IIA binding site of human serum albumin in its native, unfolded, and refolded states using small molecular probes. *J. Am. Chem. Soc.* **2008**, *130*, 10793−10801. (c) Ding, F.; Zhao, G.; Huang, J.; Sun, Y.; Zhang, L. Fluorescence spectroscopic investigation of the interaction between chloramphenicol and lysozyme. *Eur. J. Med. Chem.* **2009**, *44*, 4083−4089. (d) Johansson, J. S.; Eckenhoff, R. G.; Dutton, P. L. Binding of halothane to serum albumin demonstrated using tryptophan fluorescence. *Anesthesiology* **1995**, *83*, 316−324.

(18) Pacheco, M. E.; Bruzzone, L. Synchronous fluorescence spectrometry: Conformational investigation or inner filter effect? *J. Lumin.* **2013**, *137*, 138−142.

(19) Castiñeiras, A.; Fernández-Hermida, N.; García-Santos, I.; Gómez-Rodríguez, L. Neutral NiII, PdII and PtII ONS-pincer complexes of 5-acetylbarbituric-4N-dimethylthiosemicarbazone: synthesis, characterization and properties. *Dalton Trans.* **2012**, *41*, 13486−13495.

(20) Pettinari, R.; Marchetti, F.; Petrini, A.; Pettinari, C.; Lupidi, G.; Fernández, B.; Diéguez, A. R.; Santoni, G.; Nabissi, M. Ruthenium-(II)-arene complexes with dibenzoylmethane induce apoptotic cell death in multiple myeloma cell lines. *Inorg. Chim. Acta* **2017**, *454*, 139−148.

(21) Tang, J.; Luan, F.; Chen, X. Binding analysis of glycyrrhetinic acid to human serum albumin: Fluorescence spectroscopy, FTIR, and molecular modeling. *Bioorg. Med. Chem.* **2006**, *14*, 3210−3217.

(22) Cheng, Z. Studies on the interaction between scopoletin and two serum albumins by spectroscopic methods. *J. Lumin.* **2012**, *132*, 2719−2729.

(23) Jayabharathi, J.; Thanikachalam, V.; Venkatesh Perumal, M. Mechanistic investigation on binding interaction of bioactive imidazole with protein bovine serum albumin-A biophysical study. *Spectrochim. Acta, Part A* **2011**, *79*, 502−507.

(24) Ibrahim, N.; Ibrahim, H.; Kim, S.; Nallet, J. P.; Nepveu, F. Interactions between antimalarial indolone-N-oxide derivatives and human serum albumin. *Biomacromolecules* **2010**, *11*, 3341−3351.

(25) Ramachandran, E.; Senthil Raja, D.; Bhuvanesh, N. S. P.; Natarajan, K. Mixed ligand palladium(II) complexes of 6-methoxy-2-oxo-1,2-dihydroquinoline-3-carbaldehyde 4*N*-substituted thiosemicarbazones with triphenylphosphine co-ligand: synthesis, crystal structure and biological properties. *Dalton Trans.* **2012**, *41*, 13308−13323.

(26) (a) Shapiro, G. I.; Harper, J. W. Anticancer drug targets: cell cycle and checkpoint control. *J. Clin. Invest.* **1999**, *104*, 1645−1653. (b) Wang, D.; Lippard, S. J. Cellular processing of platinum anticancer drugs. *Nat. Rev. Drug Discovery* **2005**, *4*, 307−320.

(27) Sabharwal, S. S.; Schumacker, P. T. Mitochondrial ROS in cancer: initiators, amplifiers or an Achilles' heel? *Nat. Rev. Cancer* **2014**, *14*, 709−721.

(28) Lo, K. K. W.; Zhang, K. Y. Iridium(III) complexes as therapeutic and bioimaging reagents for cellular applications. *RSC Adv.* **2012**, *2*, 12069−12083.

(29) Boya, P.; Kroemer, G. Lysosomal membrane permeabilization in cell death. *Oncogene* **2008**, *27*, 6434−6451.

(30) (a) Li, C. Y.; Yu, M. X.; Sun, Y.; Wu, Y. Q.; Huang, C. H.; Li, F. Y. A nonemissive iridium(III) complex that specifically lights-up the nuclei of living cells. *J. Am. Chem. Soc.* **2011**, *133*, 11231−11239. (b) Puckett, C. A.; Barton, J. K. Mechanism of cellular uptake of a ruthenium poly-pyridyl complex. *Biochemistry* **2008**, *47*, 11711−11716.

DOI: 10.1021/acs.inorgchem.8b01656
Inorg. Chem. XXXX, XXX, XXX−XXX